AGU PUBLICATIONS

JGR

Journal of Geophysical Research: Space Physics

RESEARCH ARTICLE
10.1002/2016JA023121

Key Points:
- UHF radar observed enhancements in electron density with an altitude extent do not, in fact, correspond to a true increase in electron density
- The upshifting and spread of plasma lines above pump frequency shows the correlation in heating cycle with the above enhancements
- The enhancement in electron temperature occurring as a function of pump frequency around the reflection altitude of the pump

Correspondence to:
J. Wu,
wujun1969@163.com

Citation:
Wu, J., J. Wu, M. T. Rietveld, I. Haggstrom, H. Zhao, and Z. Xu (2017), The behavior of electron density and temperature during ionospheric heating near the fifth electron gyrofrequency, *J. Geophys. Res. Space Physics*, *122*, doi:10.1002/2016JA023121.

Received 28 JUN 2016
Accepted 20 DEC 2016
Accepted article online 29 DEC 2016

The behavior of electron density and temperature during ionospheric heating near the fifth electron gyrofrequency

Jun Wu[1], Jian Wu[1], M. T. Rietveld[2,3], I. Haggstrom[4], Haisheng Zhao[1], and Zhengwen Xu[1]

[1]National Key Laboratory of Electromagnetic Environment, China Research Institute of Radio Wave Propagation, Beijing, China, [2]EISCAT, Ramfjordbotn, Norway, [3]Also at UiT, Arctic University of Norway, Tromsø, Norway, [4]EISCAT Scientific Association, Kiruna, Sweden

Abstract The experimental phenomena involving the changes in electron temperature and electron density as a function of pump frequency during an ionospheric heating campaign at European Incoherent Scatter near Tromsø, Norway, are reported. When the pump frequency is slightly above the fifth electron gyrofrequency, the UHF radar observation shows some apparent enhancements over a wide altitude range in radar echo, ion line, and electron density respectively, which are apparently altitude independent and consistent temporally with the upshifting and spread of plasma line around the reflection altitude. However, they do not, in fact, correspond to true increase in electron density. Based on some existing theories, some discussions are presented to try to explain the above enhancements and the upshifting and spread of plasma line. Even so, the mechanism remains to be determined. In addition, the observation also shows some enhancements in electron temperature as a function of pump frequency around the reflection altitude of the pump, which are dependent on the behavior of dispersion of the upper hybrid wave near the fifth electron gyrofrequency.

1. Introduction

The effect of powerful radio waves (usually termed as a pump) on the ionosphere includes the development of a wide range of phenomena, the most common of which is the enhancement in electron temperature and electron density perturbations as either an enhancement or a decrease around the reflection altitude of the pump. *Gordon et al*. [1971] and *Gordon and Carlson* [1974] reported the ionospheric effect of a pump on the vertical electron temperature profile above Arecibo and showed that the stronger pump power, the more significant was the mean enhancement in electron temperature in the altitude range of 250 km to 350 km. Moreover, the enhancement in electron temperature usually takes place for an O mode pump, whereas only weak effects were observed for an X mode pump. The modulation instability of plasma waves in a magnetic field can result in some cavities filled with plasma wave, which collapse and lead to an explosive increase in the density variation when the pump is directed along the magnetic field [*Krasnosel'skikh and Sotnikov*, 1977]. *Sotnikov et al*. [1978] studied strong plasma turbulence at the lower hybrid frequency as well as the collapse of lower hybrid waves and examined the dissipation mechanisms limiting the collapse of an individual caviton and furthermore evaluated the dissipation rate of pump. *Mantas et al*. [1981] carried out a detailed study of the thermal effect of ionospheric heating on the nighttime *F* region ionosphere. It was found that the enhancement in electron temperature spread over a wide altitude range, for which heat conduction was responsible, and that about half the heating was caused by anomalous absorption and half by derivative absorption. However, later observations provided the evidence that anomalous electron heating in the presence of small-scale field-aligned irregularities dominated over collision heating at high latitude [*Robinson et al*., 1996]. At Arecibo, some large enhancements of 1000 K–2000 K in electron temperature were observed around the reflection altitude of the pump and were accompanied by small-scale field-aligned irregularities with large reductions of 10%–15% in electron density and elevated electron temperature [*Djuth et al*., 1987]. *Newman et al*. [1988] showed that the dramatically large temperature enhancement was attributable primarily to the low cooling rate of the plasma, rather than the high heating rate. *Duncan et al*. [1988] presented observations of density reductions exceeding 50% with the electron temperatures in the depletions increased by factors of 3 to 4, extending hundreds of kilometers along the geomagnetic field. These density depletions were thermally driven, that is, to say, due to the much lower cooling rate caused by poor thermal coupling. At European Incoherent Scatter (EISCAT) [*Stocker et al*., 1992], using a pump in O mode at full power, the

electron temperature increased up to 55%, whereas the measurements of electron density have revealed both enhancements and reductions around the reflection altitude of the pump. These differences were indicative of variations in the balance between the transport and chemical effects. *Honary et al*. [1993] observed electron temperature and electron density temporal fluctuations induced by pump, which indicated that the coupled electron temperature and electron density oscillation was driven by chemical perturbation. *Rietveld et al*. [2003] presented some enhancements in electron temperature of up to 3000 K, which spread along the magnetic field to an altitude of 700 km and showed a strong dependence on the angle of pump to magnetic field. The pump excited optical emission and the enhanced electron temperature were linked clearly to the same mechanism involving upper hybrid waves and small-scale irregularity [*Mantas*, 1994; *Mantas and Carlson*, 1996; *Gurevich and Milikh*, 1997; *Leyser et al*., 2000; *Bernhardt et al*., 2000; *Gustavsson et al*., 2001; *Pedersen and Carlson*, 2001; *Kosch et al*., 2002; *Kuo and Rubinraut*, 2005].

Besides Ohmic coupling directly between the pump and ionospheric plasma, the enhancement in electron temperature and the decrease in electron density are associated with artificial small-scale irregularities and anomalous absorption. *Utlaut and Violette* [1974] reported for the first time that anomalous absorption could be seen on ionograms from slightly below the pump frequency up to the *F* region critical frequency. For this reason, the anomalous absorption was originally termed as wide band absorption. As an example, on local either preexisting or artificially induced small-scale irregularities, the O mode pump can be converted into electrostatic upper hybrid waves at the altitude of the upper hybrid resonance, which propagate near perpendicular to the magnetic field and dissipate energy by being trapped in those small-scale irregularities. Thus, Ohmic heating from those trapped waves provides the necessary positive feedback for the further development of small-scale irregularities. The above process should finally lead to the anomalous absorption of the pump, furthermore, to the enhancement in electron temperature and the decrease in electron density as well as the stimulated electromagnetic emission. *Gurevich et al*. [1995] established a nonlinear theory determining the conditions for the existence and structure of the stationary small-scale irregularities induced by pump and predicted a strong enhancement in electron temperature inside the small-scale irregularities and large change of the depth of the irregularities. These effects decrease dramatically in a narrow region near the electron cyclotron resonance. Furthermore, *Gurevich et al*. [1996] constructed a nonlinear theory of anomalous absorption of a pump on small-scale irregularities. Based on this nonlinear theory, a new model of the artificial airglow was proposed [*Gurevich and Milikh*, 1997]. In 1998, considering the electron temperature measured by incoherent scatter radar, *Gurevich et al*. [1998] put forward a method to determine the enhancement in local electron temperature. With regard to the problem of the nonlinear structuring of the modified ionosphere due to the self-focusing of a pump on the bunches of small-scale irregularities, two main conditions of self-focusing, namely, propagation of pump along the magnetic field for effective excitation of small-scale irregularity and trapping of pump by large-scale irregularities, were formulated [*Gurevich et al*., 1999].

It has been found that those enhancements in electron temperature also exhibit a dependence on the difference between pump frequency and a harmonic of the electron gyrofrequency. *Mjolhus* [1993] predicted that the effect of ionospheric heating should be suppressed when the pump frequency was slightly below a harmonic of the electron gyrofrequency. This is due to the existence of a second cutoff in the upper hybrid dispersion relation. Moreover, the peculiarities of the absorption of pump near the third electron gyrofrequency were studied [*Gurevich et al*., 1996]. Some experiments were performed and have confirmed the above theories and predications. Using the EISCAT heater, an O mode pump was transmitted vertically at the frequency varying in small steps around the third electron gyrofrequency. Measurements of anomalous absorption of pump and enhancement in electron temperature all exhibited wide minima as the heater frequency in the vicinity of the third electron gyrofrequency. The results suggested that the pump could not excite the small-scale field-aligned irregularities as pump frequencies approached the third electron gyrofrequency but induce very small-scale irregularities, which were responsible for the production of fast electrons and the ionized patches [*Honary et al*., 1995]. The results given by *Robinson et al*. [1996] indicated that there were strong minima in anomalous absorption and electron temperature when pump frequency is operating in the vicinity of the third and fourth electron gyrofrequencies and that anomalous electron heating in the presence of small-scale field-aligned irregularities dominated over collision heating at high latitudes. Experimental results of resonant high-frequency scattering off small-scale field-aligned irregularities excited by a pump transmitted by the Sura radio facility in Russia also showed a minimum in the scattered signal

strength when the pump frequency was near the fourth electron gyrofrequency and a significant broadening of the frequency spectrum of the scattered signal for pump frequencies above the fourth electron gyrofrequency [*Ponomarenko et al*., 1999]. On 3 November 2000, EISCAT heater was stepped in frequency through the third electron gyrofrequency. A significant decrease in the artificial optical emission strength and Cooperative UK Twin Auroral Sounding System radar backscatter proved that upper hybrid turbulence was intimately linked to the mechanism for high-latitude artificial airglow, at least for 630 nm photons [*Kosch et al*., 2002]. *Borisova et al*. [2014, 2016] presented data including (1) the coexistence of the thermal parametric instability and parametric decay instability near the fourth gyroresonance harmonic, (2) an apparent increase in electron density by 40–50% in a wide range of altitudes, (3) a weak suppression of artificial ionospheric irregularities with transverse scales of 7.5–9.0 m during heating at a frequency near the fifth electron gyroharmonic, and (4) plasma lines ($HFPL_2$) excited at frequency higher 150–250 kHz than the pump as a result of the four-wave interaction possibly.

Here we present some further experimental results deduced from EISCAT UHF observations during ionospheric heating experiments using the EISCAT heater operated in O mode polarization and at frequencies sweeping near the fifth electron gyrofrequency on 11 March 2014. In this paper, the principal objective should be to examine electron temperature and electron density as well as their behavior in pump frequency.

2. Experiment and Observations

The EISCAT heater [*Rietveld et al*., 1993, 2016] is located at Ramfjordmoen near Tromsø, Norway (69.58°N, 19.21°E, magnetic dip angle $I = 78°$). The 12 transmitters can generate up to ~ 1.2 MW of continuous wave power in the frequency range from 3.85 to 8 MHz. There are three antenna arrays that cover the frequency ranges of 3.85–5.65 and 5.5–8 MHz, two with a gain of ~ 24 dB (dependent on frequency), which produce a beam width of 14.5° and a maximum effective radiated power (ERP) of ~ 300 MW, and one with a gain of ~30 dB resulting in a beam width of ~ 7.5°. The principal diagnostic, EISCAT UHF radar [*Rishbeth and Van Eyken*, 1993] located approximately 500 m from the EISCAT heater is an incoherent scatter radar operating at 930 MHz. The antenna is a 32 m parabolic dish with a beam width of ~ 0.5° at half maximum power. It is fully steerable in azimuth and elevation.

Using EISCAT heater and UHF radar, the experiment was conducted at 12:30–14:30 UT (universal time) on 11 March 2014. The EISCAT heater was operated in O mode at frequencies sweeping in steps of 2.804 kHz from 6.7 MHz to 7 MHz near $5f_{ce}$ as illustrated by the bottom panel of Figure 2 and some following figures, through which one can follow clearly the stepping change in pump frequency f_{HF} and see the corresponding plasma effect, where f_{ce} is the local electron cyclotron frequency at the altitude of ~ 200 km with a value of ~ 1.366 MHz in Tromsø, with a modulation cycle of 18 min on, followed by 12 min off. The period of each step frequency was 10 s, that is, 108 frequencies over a heating period of 18 min. The heating beam was field aligned (approximately 12° south of the zenith), and ERP for O mode was calculated to be in the range 56 MW–78 MW. Array 3 was used, and because of an unbalance in the number of transmitters used, there was also about 10 MW ERP of X mode radiated.

The UHF radar used "beata" modulation and started observations at 12:32:30 UT and remained field aligned, with a 12.5° zenith and 186.2° azimuth, where beata mode uses a 640 μs (32 × 20 μs) alternating code pulse with 10 μs sampling,which resulted in a undecoded ~ 96 km range resolution and a decoded ~ 2.5 km range resolution. In addition, to measure the effect induced by the pump for each step of frequency, the data were analyzed using an integration time of 10 s by version 8.7 of GUISDAP (Grand United Incoherent Scatter Design and Analysis Package) software [*Lehtinen and Huuskonen*, 1996] and version 2.67 of Real-Time Graphic.

During the experiment, the local geomagnetic condition was relatively inactive. The total magnetic strength on the ground and at the altitude of 200 km varied in the interval of **[**53452.5 nT, 53485 nT**]** and **[**49210 nT, 49240 nT**]**, respectively, from 12:30 UT to 14:30 UT, where the later was obtained from the International Geomagnetic Reference Field model by extrapolating the measurements on the ground and "**[]**" denotes the closed interval. Thus, the corresponding fifth electron gyrofrequency at the altitude of 200 km should be in the interval of **[**6.8922 MHz, 6.8964 MHz**]**, which lies in the interval of pump frequency f_{HF} **[**6.7 MHz, 7 MHz] exactly.

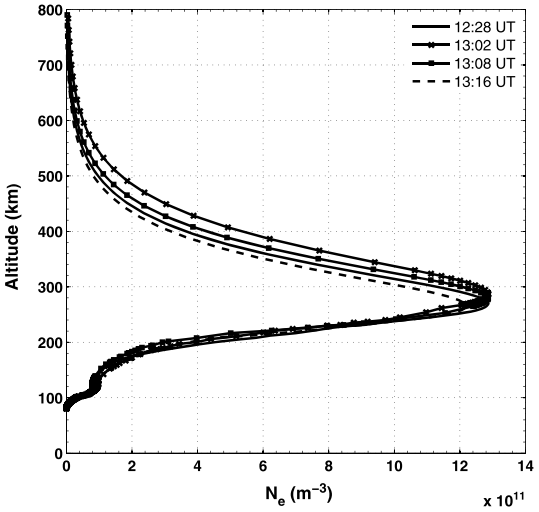

Figure 1. The electron density profile obtained by Dynasonde in EISCAT at 12:28 UT, 13:02 UT, 13:08 UT, and 13:16 UT. The profiles above the peak are an extrapolation.

In addition, the mean critical plasma frequency of ionosphere was ~ 9 MHz at the F_2 cutoff altitude of ~ 280 km from 12:30 UT to 14:00 UT and decreased to ~ 8.54 MHz from 14:00 UT to 14:30 UT. As some examples, Figure 1 shows some vertical profiles of electron density obtained through the measurement of the Dynasonde HF sounder at EISCAT before and during the experiment, which were measured at 12:28 UT, 13:02 UT, 13:08 UT, and 13:16 UT, respectively. One can see that the inactive ionosphere below the altitude of ~ 280 km and the successive slight decrease in electron density above ~ 280 km at 13:02 UT, 13:08 UT, and 13:16 UT, respectively.

Figure 2 shows the ratios of the undecoded UHF radar echo power P to their undisturbed value P_0 as a function of heating cycles within the altitude range from 76.6 km to 720 km, where P_0 is the median of the profile of the undecoded UHF radar echo over the final 5 min of the last cycle, namely, at 14:25 UT–14:30 UT. In order to facilitate the following description and discussion, it is necessary to divide the pump frequency band of **[**6.7 MHz, 7 MHz**]** into three bands, namely, the high-frequency band (HB), the gyrofrequency band (GB), and the low-frequency band (LB). For instance, we choose HB to be (6.857009 MHz, 7 MHz], GB to be **[**6.84299 MHz, 6.857009 MHz], and LB to be [6.7 MHz, 6.84299 MHz), respectively, in the third cycle, where "()" means the open interval. Indeed, due to the slight perturbation of the geomagnetic field, the above division in each cycle should be slightly different from each other.

In Figure 2, one can see two types of strong enhancements in P/P_0, the first of which occurs over the altitude range from ~ 155 km to ~ 250 km in the GB and is up to ~1.3 to ~1.5 and the second of which develops up to ~1.5 and takes place at the higher frequencies of (~6.93 MHz–7 MHz**]** in the HB, similarly, which can be termed as HHB. Unlike the first type of enhancement, the second type of enhancement appears to be

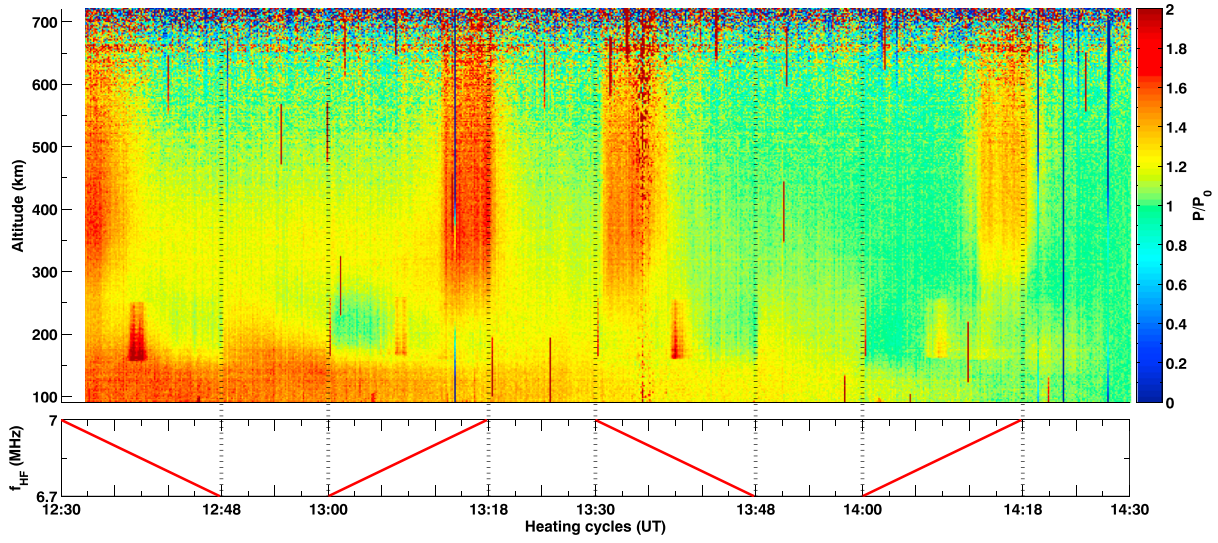

Figure 2. The ratios of UHF radar echo power from the undecoded 640 μs alternating code pulse with a height resolution of 94 km for 12.5° zenith versus heating cycles, where the black dotted vertical lines correspond to heating on and off and the red solid line the stepping change in pump frequency.

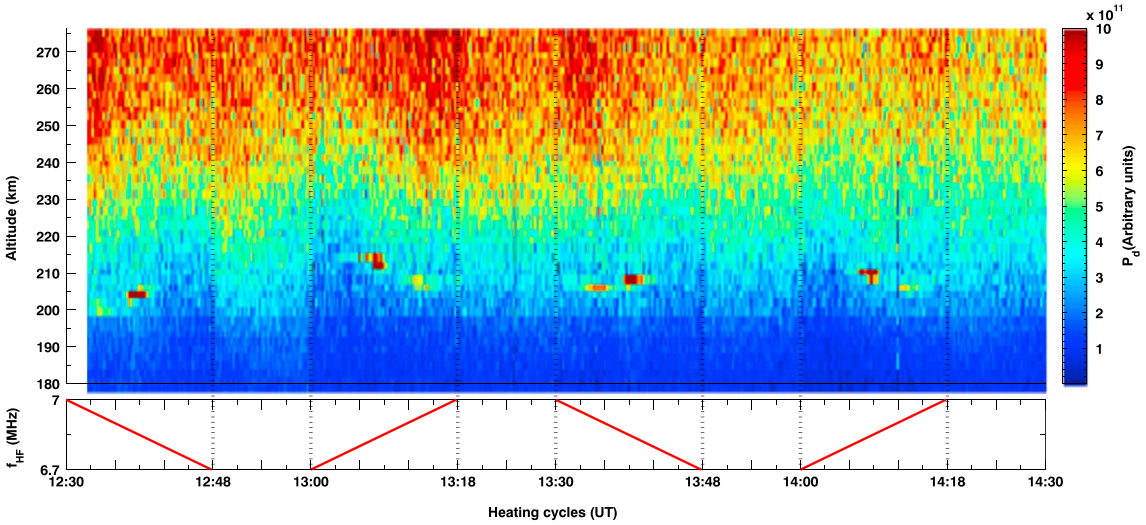

Figure 3. The UHF radar echo from the decoded pulse with a height resolution of ~2.4 km for 12.5° zenith versus heating cycles.

independent of altitude and extends from ~ 230 km to the limit of the radar's measurement above 700 km. Moreover, in the third cycle (13:30 UT–14:00 UT), it is very obvious that the enhancement does not appear immediately after the pump is switched on, but ~ 30 s later. In the second and fourth cycles (13:00 UT–13:30 UT and 14:00 UT–14:30 UT), the enhancements decay to the undisturbed level within ~ 30 s of switching off. Figure 2 also shows an enhancement in P/P_0 within the altitude range from ~ 100 km to ~ 225 km at 12:32:30 UT–13:30 UT, which is independent obviously of heating cycles and is due to the larger electron density of background ionosphere.

On the other hand, in all of heating cycles, some decreases in P/P_0 take place in the LB and within same altitude range as the first type of enhancement, which are up to ~ 0.85 and become weaker at those pump frequencies f_{HF} being closer to GB. Additionally, they appear immediately after the pump is switched on as seen in the second and fourth cycles and disappear immediately after the pump is switched off as shown in the first and third cycles.

The version 8.7 of the GUISDAP software [*Lehtinen and Huuskonen*, 1996] also gives the decoded power profile of radar echo with a height resolution of ~ 2.4 km in the altitude range of ~ 48.5 km to ~276.8 km for 12.5° zenith, which can be used to determine the reflection altitude of the pump by assuming that the pump enhanced ion line is caused by parametric decay instability. Due to the Bragg condition, a radar with frequency f_r in monostatic operation detects the propagating Langmuir wave and ion acoustic wave enhanced by the pump at the altitude [*Stubbe et al.*, 1992]:

$$z = z_0 - 12\frac{v_e^2 f_r^2}{c^2 f_{HF}^2} H, \tag{1}$$

where z_0 denotes the reflection altitude of the pump, H the scale height, v_e the thermal electron velocity, and c the velocity of light. With respect to the operating frequency of EISCAT UHF radar $f_r = 930$ MHz, the pump frequency $f_{HF} = 7$ MHz, the electron temperature $T_e \approx 2000$ K and H with the reasonable value of ≈50 km at the altitude of 200 km, then formula (1) can be expressed as $z \approx z_0 - 3.6$ km. Thus, we can identify approximatively and reasonably the reflection altitude of the pump in reference to the altitude of the pump enhanced ion line.

The decoded power profile of radar echo P_d over the altitude range of 180 km–276.8 km is presented in Figure 3, in which there are five features. (1) The reflection altitudes of the pump lie in the altitude range of ~ 200 km to ~215 km. (2) When the pump frequency f_{HF} sweeps in the GB, those strongest enhancements of $\sim 9.5 \times 10^{11}$ in P_d occur at the altitude of 204 km in the first cycle, 212 km in the second cycle, 207 km in the third cycle, and 210 km in the fourth cycle and are indeed coincident in cycle with the first type of enhancement in Figure 2. (3) When the pump sweeps in the HB, P_d is also enhanced in the altitude range of ~ 200 km to ~215 km, but much less than that in the GB. Moreover, the altitude of the enhanced P_d in the HB is lower

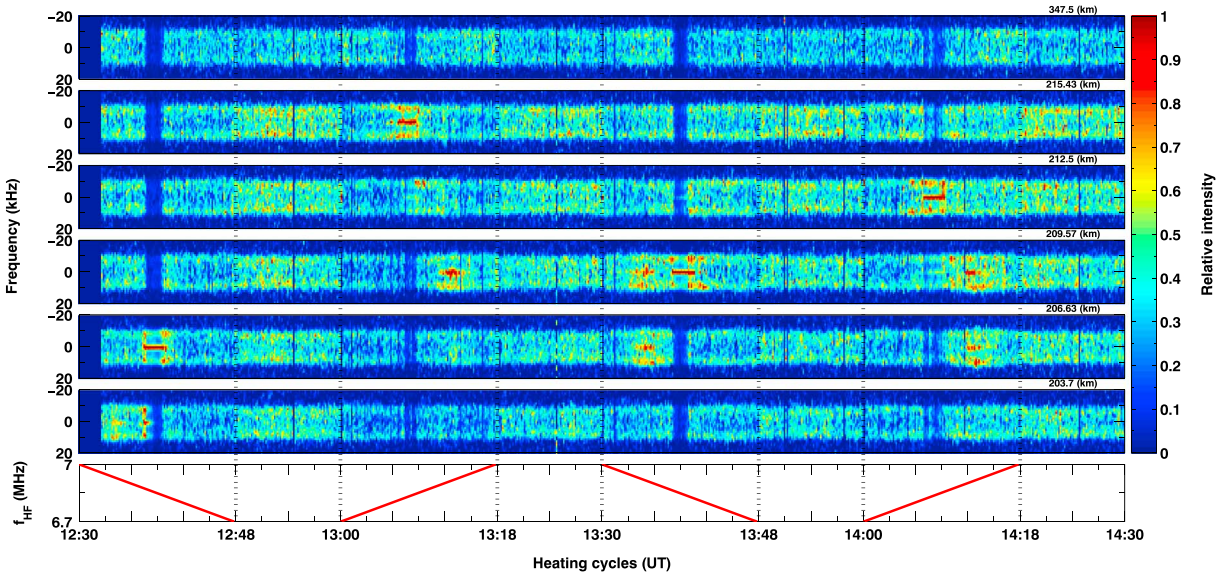

Figure 4. The ion line from −20 kHz to 20 kHz at the altitude of 203.7 km, 206.63 km, 209.58 km, 212.51 km, 215.43 km, and 347.5 km, respectively, versus heating cycles.

than that in the GB. (4) When heating in the LB, the decrease in P_d appears to be at the altitudes of ~ 190 km to ~250 km in all four cycles. (5) The most interesting are those enhancements appearing in the HHB, which only occur above the altitude of ~230 km in the first, second, and third cycles and ~240 km in the fourth cycle, whereas no apparent enhancement occurs from the reflection altitude to ~230 km.

As some examples, the ion lines within the interval of **[**−20 kHz to 20 kHz**]** at altitudes of 203.7 km, 206.63 km, 209.57 km, 212.5 km, 215.43 km, and 347.5 km are given in Figure 4, respectively. When the pump sweeps in the GB, some gaps or weak ion lines appear at those heights. They are caused by the normalization to the strongest value of ion line at any particular time. For instance, at 12:39:00 UT all of values of ion line in the interval of **[**−20 kHz to 20 kHz**]** at the altitudes of 344.56 km, 214.43 km, 212.5 km, 209.57 km, 206.63 km, and 203.7 km are normalized to the value of ion line at 0 Hz at 206.63 km. Thus, those gaps or weakening do not imply a real decrease in ion line or any unusual response.

In the HHB, the ion lines at the altitude of 347.5 km show some distinctive enhancements, which indeed correspond temporally to the enhancements in P/P_0 extending over a wide altitude range. In the HB, some strong enhancements in ion line at the altitude of 203.7 km in the first cycle, 209.57 km and 212.5 km in the second cycle, 206.63 km and 209.57 km in the third cycle, and 206.63 km and 209.57 km in the fourth cycle are very obvious. In the GB, one can see some enhancements in ion line at the altitudes of 206.63 km, 215.43 km, 209.57 km, and 212.5 km in the first, second, third, and fourth cycles respectively. The most prominent features are those significant "spikes" in the center of ion line occurring at altitudes of 203.7 km, 206.63 km, 209.57 km, 212.5 km, and 215.43 km, which are the manifestation of the oscillating two-stream instability or the purely growing instability, and the significant "shoulders" occurring at altitudes of 203.7 km, 206.63 km, 209.57 km, 212.5 km, and 215.43 km, which are the confirmation of parametric decay instability [*Stubbe et al*., 1992; *Kohl et al*., 1993]. On the other hand, there are some decreases in ion line in the LB at altitudes of 203.7 km, 206.63 km, 209.57 km, 212.5 km, and 215.43 km, which are associated obviously with those decreases in P/P_0 in the LB shown in Figure 2. In addition, one can also see some decreases in ion line in the HB at altitudes 203.7 km, 206.63 km, 209.57 km, 212.5 km, and 215.43 km. Moreover, the ion line becomes slightly wider in the period of heating on than heating off.

The previous observations at EISCAT showed that the altitude of ion line was about 3 km–5 km higher than the altitude of plasma line [*Stubbe et al*., 1992; *Kohl et al*., 1993]. Indeed, it is difficult to explain the altitude difference between the pump induced ion line and plasma line. *Stubbe et al.* [1992] and *Kohl et al.* [1993] thought it was due to the virtual observation at a frequency 933 MHz/2. Therefore, considering the above altitude difference, the downshifted plasma lines within the frequency range from −6.7 MHz to −7.25 MHz at

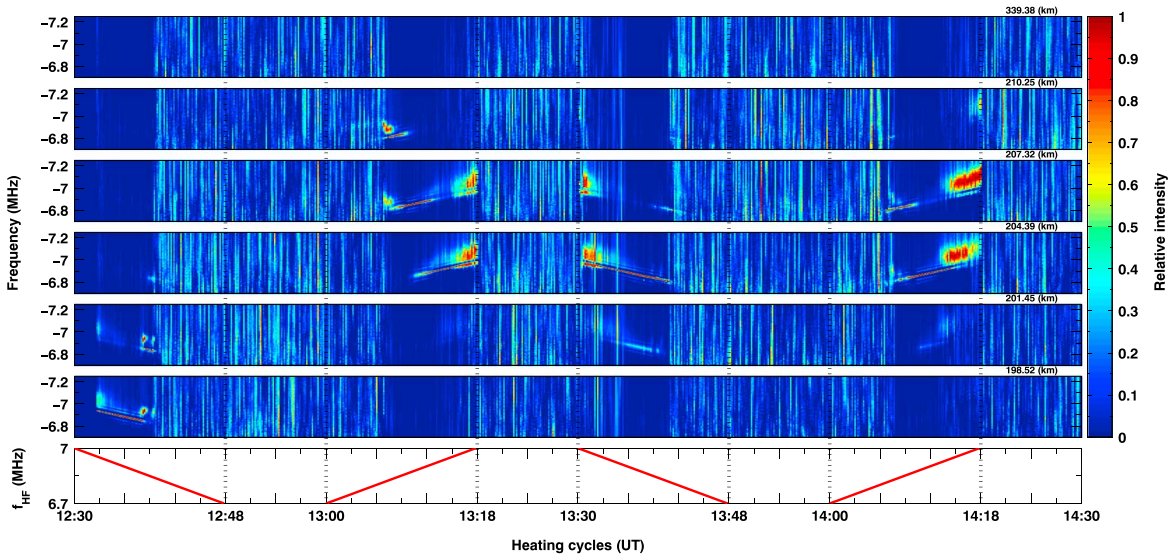

Figure 5. The downshifted plasma line at altitudes of 198.52 km, 201.45 km, 204.39 km, 207.32 km, 210.25 km, and 339.38 km, respectively, versus heating cycles.

altitudes of 198.52 km, 201.45 km, 204.39 km, 207.32 km, 210.25 km, and 339.38 km, respectively, are taken from the channel covering Doppler frequency offsets from −4.75 MHz to −7.25 MHz and shown in Figure 5. In a similar way to ion line, these plasma lines show similar gaps or weakening intervals caused by the normalization, but they occur in the GB and HB. At the altitude of 339.48 km, no pump-induced plasma line is found. At the altitudes of 198.52 km, 201.45 km, 204.39 km, 207.32 km, and 210.25 km, however, there are two "layers" of plasma lines, the lower one of which is the decay line and lies at frequency $f_{HF} - f_{ia}$, where f_{ia} is the frequency of ion acoustic wave and ~9.5 kHz here, as is expected from the parametric decay instability induced by the pump, and the upper one of which is the upshifted and spread plasma line at frequencies above the pump frequency, which occur only in the HHB at altitudes of 204.39 km and 207.32 km in the second, third, and fourth cycles, in the GB at altitudes of 198.52 km and 201.45 km in the first cycle and at altitudes of 207.32 km and 210.25 km in the second cycle. The more interesting is that the upshifting and spread of the upper "layer" of plasma line is coincident in heating cycle with those enhancements in P/P_0 over a wide altitude range. In addition, no enhancement in plasma line was observed in the LB at all altitudes. *Borisova et al.* [2016] also reported the presence of two traces of the HF-induced plasma line in the spectrograms, termed as $HFPL_1$ and $HFPL_2$, respectively.

Figure 6 (top) is the altitude profile of the ratios of electron density N_e to the undisturbed background value of N_{e0} as a function of heating cycle, where N_{e0} is taken from the median of the profile of electron density taken from the final 5 min of the last cycle of the UHF radar observations at 14:25 UT–14:30 UT. In a narrow region around the reflection altitude, it can be seen that those enhancements in N_e/N_{e0} in the GB and HB in the third and fourth cycles are up to ~1.4. In the first and second cycles, however, no apparent enhancement in N_e/N_{e0} around the reflection altitude has been seen.

In the HHB, there are some strong enhancements in N_e/N_{e0} of ~1.6, which extend from approximately the reflection altitude to ~670 km and are apparently altitude independent. The enhancement does not occur immediately when heating is turned on at 13:30 UT, but it has a delay of ~30 s and develops in the HHB and disappears with the falling f_{HF}. When f_{HF} sweeps up, the enhancement is absent in the LB and GB and appears in the HHB, and it does not disappear immediately after the heating is switched off at 13:18 UT and 14:18 UT but decays to an undisturbed level within approximately ~30 s. Figure 6 (top) also shows some enhancements in N_e/N_{e0} extending from ~100 km to ~225 km, especially at 12:30 UT–13:00 UT, which do not depend on heating cycles, but is due to the larger electron density N_e in the background ionosphere in the altitude range of ~ 100 km to ~225 km at 12:30 UT–13:00 UT.

To obtain more detailed insight into the change of electron density in the altitude, a subset of altitude profile of N_e/N_{e0} within the altitude range from 180 km to 300 km is given in Figure 6 (middle). It is evident that those

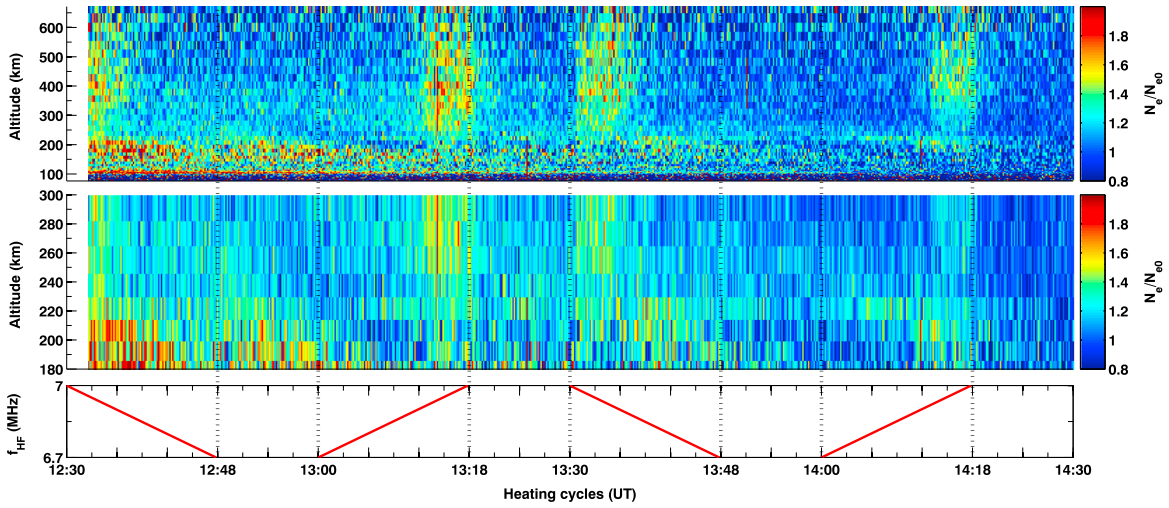

Figure 6. The ratios of N_e to N_{e0} (top) and its subset within the altitude range of 180 km–300 km (middle) versus heating cycles.

enhancements in electron density around the reflection altitude take place in the HB and GB at the altitudes of 214 km and 200 km. In the first cycle, the strongest enhancement in N_e/N_{e0} occurs at the altitude of 200 km. In the second, third, and fourth cycles, however, the strong enhancement in N_e/N_{e0} occur at the altitude of 214 km and the relative weak enhancement in N_e/N_{e0} at the altitude of 200 km.

The altitude profile of the ratios of electron temperature T_e to the undisturbed values of T_{e0} as a function of heating cycle is given in Figure 7 (top), where T_{e0} is given by the median of the profile of electron temperature taken from the final 5 min of the last cycle of the UHF radar observations. When heating on, there is a strong enhancement in T_e/T_{e0} extending in the vicinity of the reflection altitude, which varies with pump frequency f_{HF} in particular and disappears when heating off. When f_{HF} sweeps in the LB, T_e/T_{e0} enhances strongly up to ~1.5, whereas when f_{HF} lies in the HB, there is slightly less enhancement in T_e/T_{e0} of approximately up to ~1.25. When f_{HF} is in the GB and very close to $5\Omega_{ce}$ from below, T_e/T_{e0} is approximately on the order of ~1.2 and is less than that in both the LB and HB. Consequently, it is noticeable that

$$(T_e/T_{e0})_{LB} > (T_e/T_{e0})_{HB} > (T_e/T_{e0})_{GB}, \quad (2)$$

where $(T_e/T_{e0})_{LB}$, $(T_e/T_{e0})_{HB}$, and $(T_e/T_{e0})_{GB}$ indicate T_e/T_{e0} when the pump operates in the LB, HB, and GB, respectively. Similarly, a subset of altitude profile of T_e/T_{e0} within the altitude range from 180 km to 300 km

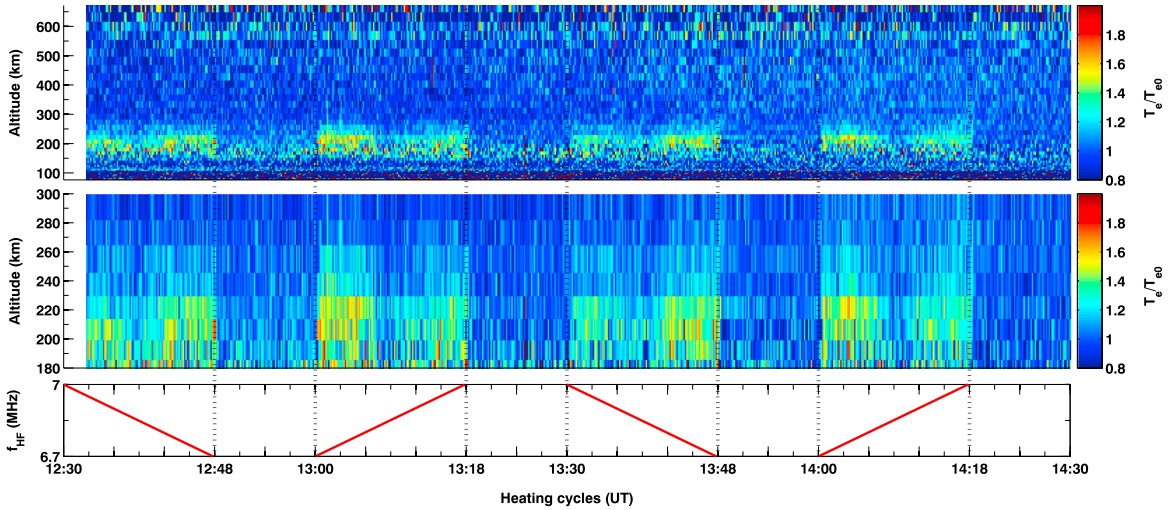

Figure 7. The ratios of T_e to T_{e0} (top) and its subset within the altitude range of 180 km–300 km (middle) versus heating cycles.

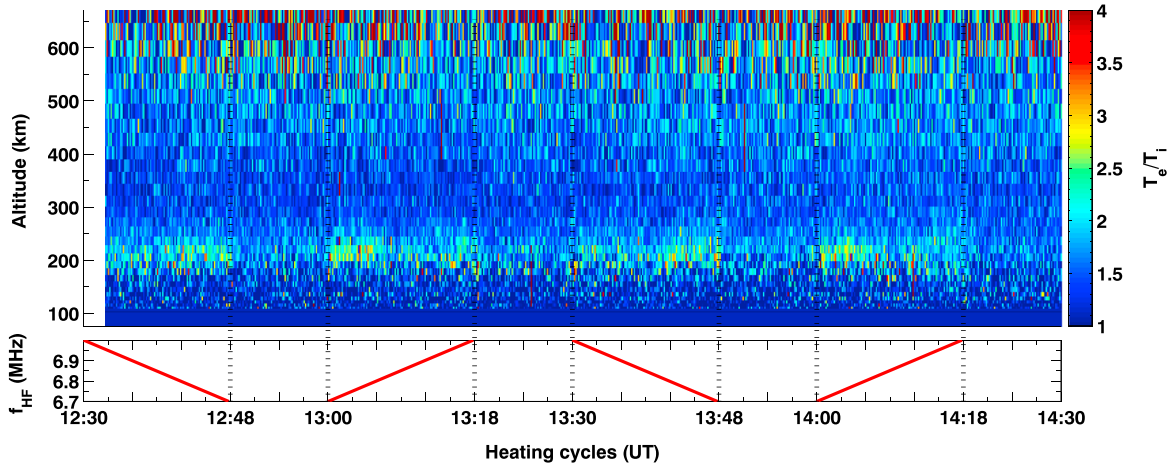

Figure 8. The altitude profile of T_e/T_i versus heating cycles.

is shown in Figure 7 (middle), which shows the strongest enhancement in T_e/T_{e0} takes place at the altitude of ~200 km and the second strongest at the altitude of ~214 km.

Figure 8 is the altitude profile of the ratios of electron temperature T_e to the ion temperature T_i as a function of heating cycle, in which there is no evidence of a change in T_e/T_i except for within the altitude range from ~186 km to ~246 km. When heating is on, there is a strong enhancement in T_e/T_i extending near the reflection altitude, the intensity of which varies with pump frequency f_{HF}. When f_{HF} lies in the LB, T_e/T_i enhances strongly up to ~2.5, whereas when f_{HF} is in the HB, there is slightly less enhancement in T_e/T_i up to ~2. In the GB, T_e/T_i is approximately on the order of ~1.65 and is less than that in both the LB and HB, namely,

$$(T_e/T_i)_{LB} > (T_e/T_i)_{HB} > (T_e/T_i)_{GB}, \tag{3}$$

where $(T_e/T_i)_{LB}$, $(T_e/T_i)_{HB}$, and $(T_e/T_i)_{GB}$ indicate T_e/T_i in the LB, HB, and GB, respectively.

3. Discussion

3.1. Radar Echo

The intensity of scattered echo P off a particular unite volume of scatter can be expressed as the product of the electron density N_e and the effective electron scattering cross-section σ_{eff} [*Djuth et al.*, 1987; *Duncan et al.*, 1988], namely,

$$P \propto N_e \sigma_{eff}, \tag{4}$$

where $\sigma_{eff} \approx \sigma_e(1 + T_e/T_i)^{-1}$ for $\frac{4\pi\lambda_D}{\lambda} \approx 0.04 \ll 1$, σ_e is the Thomson cross section of electron, and the local plasma Debye length $\lambda_D = 69\sqrt{T_e/N_e} \sim 10^{-3}$ m for a classic ionosphere [*Baumjohann and Treumann*, 1997], $\lambda = 0.32$ m for EISCAT UHF radar wave.

Comparing Figure 2 and Figure 3 with Figure 6 and Figure 8, one can find that (1) the first type of enhancement in P/P_0 is associated with both the slight enhancement in T_e/T_i and the enhancement in N_e/N_{e0}, where the enhancement in N_e/N_{e0} is deduced from an enhancement of ion line excited by oscillating two-stream instability and parametric decay instability, rather than the true increase in electron density. (2) The decrease in P/P_0 taking place over the altitude range of ~155 km to ~250 km in the LB has contributions from the enhancement in T_e/T_i. (3) We cannot see the prominent enhancement in P/P_0 near the reflection altitude in the HB, but there are some enhancements in N_e/N_{e0} at the altitude from ~200 km to ~230 km and some enhancements in T_e/T_i near the reflection altitude of the pump. Essentially, the competitive balance between the enhancement in ion line and T_e/T_i leads to no obvious decrease or enhancement in P/P_0 near the reflection altitude of the pump in the HB. Indeed, here it should be stressed that the enhancements in N_e/N_{e0} at the altitude from ~200 km to ~230 km do not correspond to the true increase in N_e but to the enhancements in ion line excited by oscillating two-stream instability and parametric decay instability. (4) Considering the second type of enhancement in P/P_0 over a wide altitude range in the HHB, however, it can be seen that

they are not associated with the enhancement in T_e/T_i but involve only the enhancements apparently in N_e/N_{e0} extending from ~ 230 km to the limit of radar measurement. From the first panel of Figure 4, one can find the consistency between ion line in the HHB at the altitude of 347.5 km and the second type of enhancement in P/P_0, which implies that the second type of enhancement in P/P_0 still is due to the enhancement in ion line. In the HHB, however, no obvious enhancement in plasma line and spikes and shoulders can be seen in Figures 5 and 4 (first panels), respectively. This implies that oscillation two-stream instability and parametric decay instability do not take place at the altitude from ~230 km to the limit of radar measurement. Then what is the process leading to those enhancements in ion line at the altitude from ~230 km to the limit of radar measurement?

It should be emphasized that those enhancements in P/P_0 are indeed induced by the enhancement in ion line in the HHB rather than natural, which implies that the pump energy upward or the increase in the energy density of the backscattered radar wave in the wide altitude range.

There are two possible ways for transporting pump energy upward when heating. One possible way is that the pump is coupled to the Z mode near the critical angle and propagates upward until it reaches the altitude of $X = 1 + Y$, where $X = f_{pe}/f_{HF}$, $Y = f_{ce}/f_{HF}$, and $f_{ce} = eB/2\pi m$, B is the magnetic field intensity, and e and m are the electron charge and mass, respectively. With regard to the experiment conducted at 12:30 UT–14:30 UT on 11 March 2014, however, $X = 1 + Y$ varies from ~1.2 for $f_{HF} = 6.7$ MHz to ~1.19 for $f_{HF} = 7$ MHz, where the critical plasma frequencies correspond to 8.05 MHz and 8.35 MHz, respectively. Considering the ionospheric background, it is not possible that the pump in Z mode can reach an altitude of ~280 km and above. In addition, *Mjolhus and Fla* [1984] have calculated the resonance spatial region (radio window) of Z mode for the EISCAT heater case, which is very localized and displaced horizontally ~15 km to ~20 km southward from the point where the pump is when it arrives at the altitude of $X = 1$. Thus, the UHF radar with a beam width of ~0.5° cannot probe the Z mode resonance region. Besides, the enhancement in N_e/N_{e0} over a wide altitude range occurs only in the HHB.

In addition, a linear mode conversion of ordinary wave into an upper hybrid wave and Bernstein wave can take place at the upper hybrid resonance altitude when heating the ionosphere. However, upper hybrid waves and Bernstein waves propagate in the directions perpendicular to the magnetic field and cannot transport heating energy upward. Therefore, the way to transport pump energy upward in a wave mode should be ruled out.

The other possible way to transport energy upward is a plasma transport process, such as diffusion along the magnetic field due to thermal pressure and density gradient. Neglecting the natural electric field and the natural wind field and only considering the thermal pressure gradient and density gradient caused by the ionosphere heating as well as gravity, the plasma diffusion velocity yields [*Risthbeth and Owen*, 1969]

$$-W_d = D\left[(1/N_e)(\mathrm{d}N_e/\mathrm{d}h) + \left(1/T_p\right)\left(\mathrm{d}T_p/\mathrm{d}h\right) + 1/H\right] \tag{5}$$

here D is the plasma diffusion coefficient and is given by $D \approx (2 \times 10^{19}/n)\mathrm{cm}^2/\mathrm{s}$ for reasonable daytime conditions, the neutral density n is given by $n[\mathrm{O}] = (5 \times 10^9)\mathrm{cm}^{-3}$, H is plasma scale height and ~50 km, and plasma temperature T_p is defined by $T_p = (T_e + T_i)/2$. It should be emphasized that the parameters used here are measured either in unmagnified plasma or along the geomagnetic direction, so the diffusion process does not take the effect of the magnetic field as well as horizontal diffusion into account. The parameters obtained during the experiment focused in this paper show $(D/H)(\mathrm{d}N_e/\mathrm{d}h) \approx 0.0025$ km/s, $(D/T_e)(\mathrm{d}T_e/\mathrm{d}h) \approx -0.0012$ km/s and $D/H_p \approx 0.0024$ km/s, then $W_d \approx -0.0037$ km/s at the reflection altitude, where the negative sign indicates the downward direction of diffusion along the magnetic field. Besides, the observation that the enhancement in P/P_0 does not immediately occurs with heating on, but a delay of ~30 s, shows the measured characteristic time of electron density enhancement is much less than the diffusion time obviously. Then the diffusion along the magnetic field due to thermal pressure and density gradients fails to support the way to transport energy upward.

A way to transport energy upward, the thermal instability excited by the pump, was given by *Kuo and Djuth* [1988]. The thermal source for the thermal instability is maintained by the pump and distributed locally near the reflection altitude of the pump and must be distributed over a large volume through heat conduction along the magnetic field. The perturbation on local electron temperature modifies the local heat conduction. As a result, the net heat flow into the perturbed region from the heat source, which is located at a different

region and also perturbed and give rise to a positive feedback to the perturbation. When the threshold of the ratio of the electron temperature to ion temperature T_e/T_i is satisfied during heating, a broad spectrum of density irregularities will be generated at the reflection altitude of the pump and flow upward along the magnetic field, furthermore, enhance the backscattering of the radar wave in a wide range of height and produce spread *F* on the ionogram trace possibly. In the experiment studied in this paper, the ratio of the electron temperature to ion temperature in the HHB $(T_e/T_i)_{\mathrm{HHB}}$ is up to ~2, which satisfy obviously the threshold for a typical ionosphere given by *Kuo and Djuth* [1988, Figure 1], then irregularities with scale sizes of ~13 m should be generated by the thermal instability with a normalized growth rate of ~0.72 [*Kuo and Djuth*, 1988, Figures 1 and 2]. Considering the normalization factor $\nu_{ei0}(m_e/m_i) = 1.7 \times 10^{-2}$ Hz [*Kuo and Djuth*, 1988], a growth time of ~82 s should be obtained, which is on timescales of the order of tens seconds and consistent approximately and reasonably with the delay of ~30 s of the enhancement in P/P_0 after heating on. However, one cannot see the similar enhancement in the LB, where $(T_e/T_i)_{\mathrm{LB}}$ is up to ~2.5 and satisfies the threshold of the thermal instability. In addition, no spread *F* was observed on the ionogram trace measured by the EISCAT Dynasonde during the experiment. Indeed, only irregularities polarized in the meridian plane can effectively cause spread *F* [*Kuo et al*., 1985; *Kuo and Djuth*, 1988]. Though the excited thermal instability cannot explain the enhancement in P/P_0 over a wide altitude range in the HHB, it provides an alternative modification of experiment in the future, namely, to suppress the enhancement in T_e/T_i by shortening the heating period of each pump frequency.

Apart from transporting pump energy upward by means of pump wave conversion and plasma transport process, we should also consider the radar wave rather than only the pump. *Rietveld and Senior* [2015] suggested a hypothesis where the field-aligned irregularities that are much larger than the radar wavelength, and perhaps with hundreds of meters scale size, cause radar waves near grazing incidence to be reflected. If the irregularities are extended long enough along the field line, multiple reflections can occur so that the region of irregularities acts as a duct where the overall decrease of the radar's field strength with distance falls off more slowly than r^2, where *r* is the propagating distance. It is this slower decrease of the radar wave with distance than the free space falloff as r^2 assumed in the normal incoherent scatter analysis that causes the stronger backscatter from all ranges above the ducting region of irregularities. Thus, an apparent enhancement in electron density can be obtained by the standard analysis of the incoherent scattering spectrum. Some evidence supporting the above hypothesis seems to be the upper layer of plasma lines in the panels of 204.39 km and 207.32 km in Figure 5, which show the coincidence in heating cycle with those enhancements in P/P_0 over a wide altitude range and must be an important clue in explaining the enhancement in P/P_0 over a wide altitude range. So far, three questions arise. (1) If the returned power to the radar is increased, not only ion line but also plasma line should be enhanced. However, the downshifted plasma line at altitude of 339.38 km does not show an enhancement in intensity. (2) Whether the large-scale irregularities can focus or collimate the radar wave at the frequency of 930 MHz. (3) What mechanism is responsible for those large-scale irregularities, which are not so easily observed because there are no suitable radars that can observe the large-scale irregularities perpendicular to the magnetic field. It seems there remains much work to be done in the future.

3.2. Plasma Line

During the ionospheric heating experiment, the enhancements in plasma line and ion line are regularly observable by incoherent scatter radar and contributed to the parametric decay instability and the oscillation two-stream instability excited by the pump. In the three-wave interaction, a strong wave $(\omega_0, \mathbf{k}_0)$ causes the growth of two weak waves $(\omega_1, \mathbf{k}_1)$ and $(\omega_2, \mathbf{k}_2)$, where the wave parameters satisfy the matching conditions, $\omega_0 = \omega_1 + \omega_2$ and $\mathbf{k}_0 = \mathbf{k}_1 + \mathbf{k}_2$. With regard to the parametric decay instability, $(\omega_0, \mathbf{k}_0)$, $(\omega_1, \mathbf{k}_1)$, and $(\omega_2, \mathbf{k}_2)$ are associated with the pump, Langmuir wave and ion acoustic wave, and to the oscillating two-stream instability, the pump interacts with a Langmuir wave of equal frequency together with an ion acoustic wave which is spatially period but has zero frequency, namely, $\omega_2 = 0$. In Figure 5, the lower layers of plasma line lie at frequency $f_{\mathrm{HF}} - 9.5\mathrm{k}$ Hz, as is expected from the parametric decay instability. Moreover, Figures 4 and 5 show that the ion acoustic wave and Langmuir wave enhanced by the parametric decay instability and the oscillation two-stream instability can travel downward and be seen below the reflection altitudes of the pump, where the radar Bragg condition $|\mathbf{k}| = 2|\mathbf{k}_r| \approx 39\ \mathrm{m}^{-1}$ is satisfied, where k*r* is wave number of radar wave.

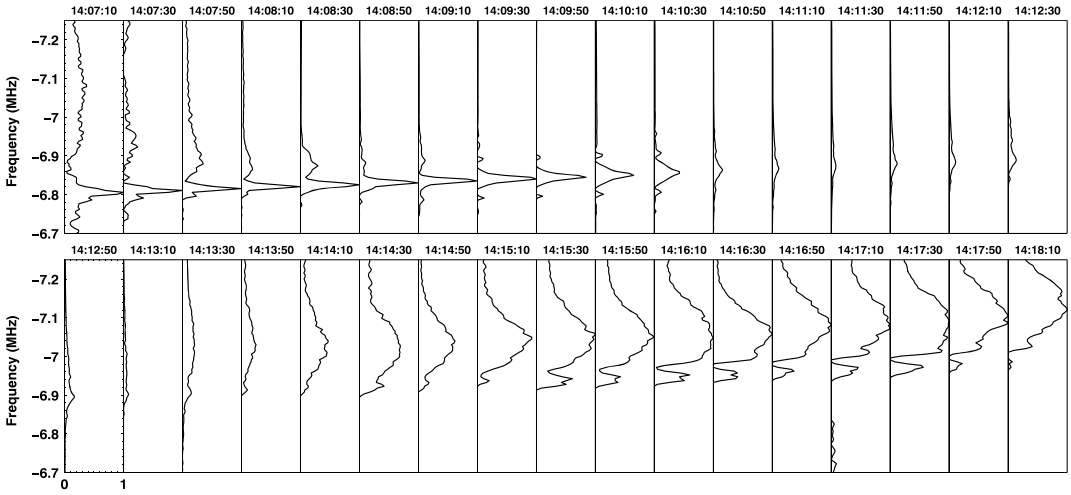

Figure 9. The downshifted plasma line from −6.7 MHz to −7.25 MHz at the altitude of 207.32 km from 14:07:10 UT to 14:18:10 UT.

The intensity of the pump has to exceed the thresholds of the parametric decay instability and the oscillation two-stream instability, respectively [*Robinson*, 1989; *Bryers et al*., 2013:]

$$E_{\mathrm{tp}} = \sqrt{4N_{e0}k_B T_i \nu / \left(\varepsilon_0 \omega_{pe} B_{\max}\right)} \tag{6}$$

$$E_{\mathrm{to}} = \sqrt{\left[4\left(1+\frac{T_e}{T_i}\right)N_{e0}k_B T_i \nu\right] / \left(\varepsilon_0 \omega_{\mathrm{pe}}\right)} \tag{7}$$

to overcome such saturation process as collision, where T_i, ν, and k_B are the ion temperature, electron collision frequency, and the Boltzmann constant, $B_{\max}$ a function of T_e/T_i and with a value of ~0.56 for $T_e/T_i = 2$ [*Stubbe et al*., 1984]. During the experiment focused in this paper, the UHF radar measured T_i, T_e/T_i, and ν at the altitude of 200 km are ~1000 K, ~1.95, and ~10 Hz, respectively, then $E_{\mathrm{tp}} \approx 0.036$ V/m and $E_{\mathrm{to}} \approx 0.046$ V/m can be obtained. For the pump in free space, the electric field E(V/m) at a range R(km) from a transmitter with ERP(kW), are given by $E \approx 0.25\sqrt{\mathrm{ERP}}/R$ [*Rietveld et al*., 1993]. Considering the pump with ERP $\approx 6 \times 10^4$ kW in the focused experiment, the electric field E should be ~0.3 V/m at the altitude of $R = 200$ km. It is obvious that the thresholds of the parametric decay instability and the oscillation two-stream instability should be satisfied by the pump.

In the following, let us examine the upper layer of plasma line, which show the upshifting from the pump frequency f_{HF} and the unstructured frequency spread. For more detailed analysis, some typical downshifted plasma lines at the altitude of 207.32 km from 14:07:10 UT to 14:18:10 UT are extracted from Figure 5 and shown in Figure 9. One can see in Figure 9 that the upshifting and spread of plasma line starts to develop at 14:13:30 UT and grows with the pump frequency f_{HF} stepping up. Additionally, the maxima of their intensity always lie at frequency $-(f_{\mathrm{HF}} + 0.1)$ MHz approximately and in the frequency range of ~−6.9 MHz to ~−7.15 MHz.

Borisova et al. [2016] gave a possible explanation of the upper layer of plasma lines (HFPL_2), namely, the possibility of interaction of four plasma waves in the region of the development of a parametric decay instability at the altitudes of $z_0 \approx z_{\mathrm{UH}}$, where z_{UH} the upper hybrid resonance altitude. At the reflection altitude, a longitudinal plasma wave excited at frequency of $f_{p1} \approx f_{\mathrm{HF}} \cos(12^{\circ})$ for 12° zenith of the heating beam, a transverse upper hybrid wave at frequency f_{UH}, and transverse Bernstein wave at frequency f_B are assumed, then a three-wave interaction may result in a fourth longitudinal plasma wave at frequency f_{p2}, and satisfy

$$f_{\mathrm{B}} + f_{\mathrm{UH}} = f_{p1} + f_{p2}. \tag{8}$$

As an example, considering the observation at 14:17:30 UT in Figure 9, we have $f_{\mathrm{HF}} = 6.994393$ MHz, $z_0 \approx 214.7$ km obtained through formula (1), $f_{\mathrm{ce}} \approx 1.38$ MHz, where the total magnetic strength at the altitude of 200 km was obtained from the International Geomagnetic Reference Field model by extrapolating the

measurements on the ground recorded at 14:17:30 UT by Tromsø Geophysical Observatory, UiT, the Arctic University of Norway, and $f_{pe} \approx 7.1$ MHz measured by UHF radar at 14:18 UT at the altitude of 214.4 km. Thus, $f_B \approx 5f_{ce} = 6.9$ MHz, $f_{UH} = 7.23$ MHz, $f_{p1} \approx 6.84154873$ MHz, and $f_{p2} \approx 7.29$ MHz can be obtained. Obviously, $f_{p2} - f_{HF} \approx 0.29$ MHz, which is not in agreement with the upshifting of plasma line of ~0.1 MHz. Indeed, *Borisova et al*. [2016] emphasized that the excitation of the upshifted plasma line ($HFPL_2$) remained open and required further research.

Based on the Zakharov model, *DuBois et al*. [1988, 1990, 1991, 1993] developed a scenario, strong Langmuir turbulence (SLT). SLT may be excited for the pump slightly above the threshold for parametric instabilities near the reflection altitude of the pump, where the ponderomotive force contains a zero-frequency component. The zero-frequency component of the ponderomotive force drives electrons out of regions of high electric field into regions of low electric field and creates a cavity in electron density, which can trap Langmuir wave. Thus, the cavity becomes deeper, and at the same time the whole cavity is compressed by the steep pressure gradient of the plasma and collapses. The spatial scale of the cavity becomes much less than a meter. Finally, the cavity bums out and induces super thermal electrons; furthermore, the local electron temperature is enhanced. The enhancement in electron temperature increases the value of the second term $3k^2 v_e^2$ of the dispersion relation of free Langmuir wave:

$$\omega_f^2 = \omega_{pe}^2 + 3k^2 v_e^2 + \Omega_{ce}^2 \sin^2(\theta), \tag{9}$$

where k is the wave number, v_e the electron thermal velocity, $\Omega_{ce} = 2\pi f_{ce}$, and θ the angle between the magnetic field and the Langmuir wave. Thus, a free Langmuir wave at ω_f being larger than the pump frequency by the order of several kilohertz may be observed as the upshifted plasma line. Moreover, the superimposing of free Langmuir waves from the various altitudes or the altitude integration results in the spread of plasma line. Similarly, the observation at 14:17:30 UT in Figure 9 will be considered as an example. We have $T_e = 2483$ K and $k = 2k_r$, where k_r denotes the wave number of the radar wave with a value of 19.6 m^{-1} for the EISCAT UHF radar, then $f_f - f_{HF} \approx 0.46$ MHz is obtained, which is not in agreement with the observation, where $f_f = \omega_f/2\pi$. Additionally, the other distinct feature suggested by *DuBois et al*. [1988, 1990, 1991, 1993], the broad caviton continuum below the pump frequency due to rapidly collapsing trapped Langmuir wave, was not be found in Figure 9. Moreover, when wave propagates in a nonuniform but stationary medium, its frequency will not change, but the wave number will change. In other words, with regard to formula (9), the change in ω_{pe} and v_e will be compensated by k to keep ω_f unchanged. However, the model suggested by *DuBois et al*. [1988, 1990, 1991, 1993] neglects the change in the wave number k and argues that the upshifting and spread of plasma line is only due to the enhancement in electron temperature.

Kuo and Lee [1992] proposed a mechanism generating HF-induced plasma lines (HFPLs) with the upshifted frequency by several tens of kilohertz, through which the parallel propagating Langmuir wave $(\omega_1, \mathbf{k}_1)$ generated by the parametric decay instability excited by the pump near the reflection height scatters into Langmuir wave $(\omega_2, \mathbf{k}_2)$ off the background lower hybrid density fluctuations $(\omega_3, \mathbf{k}_3)$ propagating in a direction perpendicular to magnetic field and generated by parametric excited Langmuir waves near the reflection height [*Kuo and Lee*, 1999], where the frequency and wave number matching conditions satisfy $\omega_1 = \omega_2 + \omega_3$ and $\mathbf{k}_1 = \mathbf{k}_2 + \mathbf{k}_3$. In Figure 9, one can see that the spreading and upshifted plasma line in the HHB are consistent temporally with the slight decrease in intensity of the decay line, which seems to imply a coupling between the upshifted plasma line and the decay line excited by the parametric decay instability, namely, an energy transfer from the decay line to the upshifted plasma line. In addition, UHF radar detected simultaneously both the upshifted Langmuir wave and the Langmuir wave excited by the parametric decay instability, then it is safe to conclude that the upshifted Langmuir wave has same wave number of 39 m^{-1} as the Langmuir wave excited by the parametric decay instability, namely, $\mathbf{k}_1 = \mathbf{k}_2$, which implies that a lower hybrid oscillation (ω_3,0) exist according to wave number matching condition $\mathbf{k}_1 = \mathbf{k}_2 + \mathbf{k}_3$. Here we still take the observation at 14:17:30 UT in Figure 9 as an example. Considering atomic oxygen as the most common ion species at the F_2 layer and using the proton-to-electron mass ratios $m_i/m_e \approx 1836$ [*Najmi et al*., 2016], $f_{ci} \approx 3.4 \times 10^{-5} f_{ce}$, $f_{pi} \approx 0.006 f_{pe}$, then the lower hybrid oscillation frequency $f_{LH} \approx 31.5$ kHz is obtained through [*Najmi et al*., 2016] the following:

$$f_{LH}^2 = \left[f_{pi}^{-2} + (f_{ce} f_{ci})^{-1} \right]^{-1}, \tag{10}$$

where m_e, m_i, f_{ci}, and f_{pi} are electron mass, ion mass, ion gyrofrequency, and ion plasma frequency. Thus, it seems possible that the lower hybrid oscillation with wide spectrum contribute to the upshifting and spread of plasma line. In addition, the cascade, a means to dissipate the parametric decay instability excited by the pump, may play a role in the spreading plasma line [*Kuo and Lee*, 1999; *Kuo*, 2001]. On the other hand, that the maxima of the spreading and upshifted plasma line always lie at frequency $-(f_{HF}+0.1)$ MHz approximately, does not confirm the conclusion given by *Kuo and Lee* [1992] that the amount of upshifted frequency is inversely proportional to the pump frequency.

A question shared by the above three mechanisms is why the spreading and upshifted plasma line appears only in the HHB, rather than in such pump band as GB and LB. Indeed, due to the coincidence of the spreading and upshifted plasma line with the enhancements in radar backscatter over a wide range, the spreading and upshifted plasma line may be an important clue in explaining those backscatter enhancements.

3.3. Electron Density

The change in electron density induced by powerful pump is difficult to measure for the following reasons. The density is much more variable both in time and space, and the artificial density change is relatively small [*Rietveld et al*., 2003]. Thus, are those apparent enhancements in N_e/N_{e0} shown in Figure 6 the true increases in electron density? Those remarkable enhancements in N_e/N_{e0} around the reflection altitude occurring in the GB in the third cycle and in the HB and GB in the fourth cycle, respectively, in Figure 6 appear to be consistent with the behavior of ion line shown in Figure 4. Thus, according to standard analysis of incoherent scattering spectrum, the apparent enhancements in N_e/N_{e0} in the GB and HB around reflection altitude should be the result of an enhancement of ion line excited by oscillating two-stream instability and parametric decay instability around the reflection altitude [*Stubbe et al*., 1992]. In other words, they do not correspond to the true increase in electron density. In addition, in the first and second cycles, one cannot see the similar enhancement in N_e/N_{e0}. This could be due to the short integrating time and the background ionosphere with the higher electron density, especially in the first cycle, which conceals those enhancements in N_e/N_{e0} induced by the enhanced ion line excited by the oscillating two-stream instability and parametric decay instability.

Considering the enhancement in N_e/N_{e0} over a wide altitude range in the HHB, however, the above interpretation is hard to explain the behavior of ion line at the altitude of 344.56 km illustrated by the first panel of Figure 4, in which no spikes and shoulders were found. *Blagoveshchenskaya et al*. [2011a, 2011b] reported EISCAT UHF radar observation of an increase up to 30% in electron density over a wide altitude range induced by an X mode pump wave with frequency $f_{HF} \approx f_xF_2$, where f_xF_2 is the critical frequency of the extraordinary wave for F_2 region. *Senior et al*. [2013] showed that the apparent large electron density enhancements over a wide altitude range do not, in fact, correspond to the true increase in electron density and may be due to some unknown mechanism that does not involve a change in plasma density but rather pump induced incoherent scatter ion line enhancement. In addition, *Borisova et al*. [2016] presented an apparent increase in electron density by 40–50% in a wide range of altitudes 450 km–500 km during O mode pump wave near fifth gyrofrequency. The enhancements in N_e/N_{e0} presented in Figure 6 have similarities to that given by *Blagoveshchenskaya et al*. [2011a, 2011b], *Senior et al*. [2013], and *Borisova et al*. [2016]. In the first place, they extend from the reflection altitude to the limit of the radar's measurement. Second, they appear to be approximately independent of altitude. Third, after the pump is switched on, they do not occur immediately but have a delay of ~30 s. Fourth, after the pump is switched off, the enhancement decays to the undisturbed level within tens of seconds. Fifth, they are not confirmed by the incoherent scatter plasma line but only involve the enhancement in ion line.

In summary, it seems reasonable to conclude that those enhancements in N_e/N_{e0} over a wide altitude range do not, in fact, correspond to a true increase in electron density, but due to the enhancement in ion line or the enhancement in radar backscatter induced by some unknown mechanism, which do not involve a change in plasma density

On the other hand, there is a slight decrease in N_e/N_{e0} around ~200 km when heating in the LB in the first cycles, which is coincident in heating cycle with the decreases in P/P_0 and P_d shown in Figures 2 and 3, respectively, and should be a result of the trapping of upper hybrid wave excited by pump at upper hybrid resonance altitude [*Mjolhus*, 1993]. As is well known, an O mode pump can couple through either preexisting

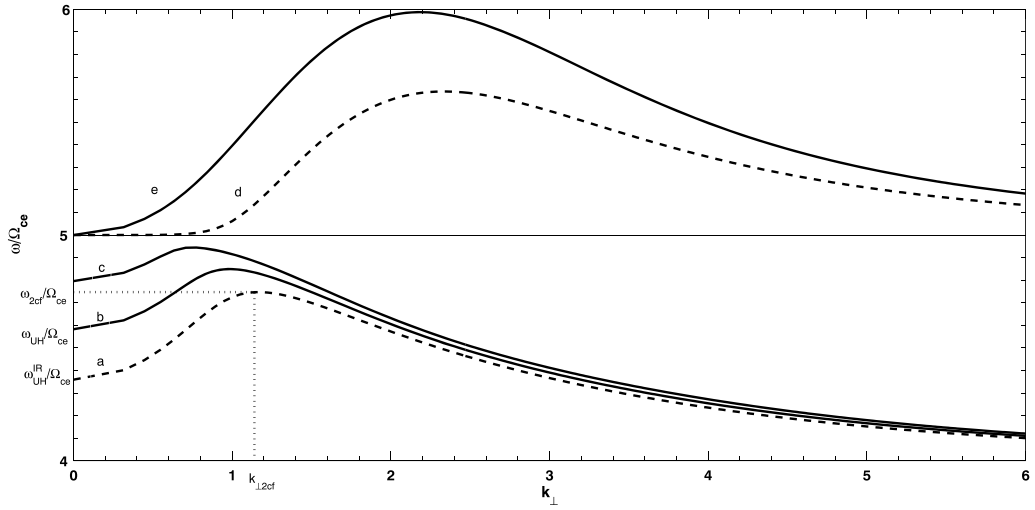

Figure 10. The schematic of dispersion curves of upper hybrid wave in the bands of $\omega/\Omega_{ce} = 4$ and $\omega/\Omega_{ce} = 5$.

or artificially induced irregularity into an upper hybrid wave at upper hybrid resonance altitude [*Dysthe et al*., 1982; *Mjolhus*, 1993; *Rietveld et al*., 2003], where pump frequency yields

$$\omega_{HF} = \omega_{UH} = \sqrt{\omega_{pe}^2 + \Omega_{ce}^2}, \tag{11}$$

here ω_{UH} denotes the upper hybrid frequency. In other words, at upper hybrid resonance altitude, the pump may excite the upper hybrid resonance in background ionosphere, which may be linearly converted into the upper hybrid wave at the edge of the irregularity and propagate into the irregularity along the gradient of electron density ∇N. The upper hybrid wave dissipates energy through Ohmic, heats electrons in the irregularity, and leads to an effect of reducing electron density in the irregularity due to thermal electron transport.

The ionospheric heating will generate a broad spectrum of density irregularities in the heated region [*Kuo et al*., 1983], which may bring about an averaging effect for the radar observation. For the sake of simplicity, here we assume an individual irregularity N_1 with a constant initial upper hybrid frequency ω_{UH}^{IR} and the second cutoff frequency ω_{2cf} [*Mjolhus*, 1993]. For the clear descriptions, Figure 10 gives the schematic of dispersion curves of upper hybrid wave in the bands of $\omega/\Omega_{ce} = 4$ and $\omega/\Omega_{ce} = 5$, which are computed for an individual irregularity density of $5.63 \times 10^9/m^{-3}$ and three background plasma densities of $6.25 \times 10^9/m^{-3}$, $6.88 \times 10^9/m^{-3}$, and $7.5 \times 10^9/m^{-3}$, respectively, where the electron gyrofrequency Ω_{ce} and electron temperature T_e are put 1 MHz and 1500 K. Additionally, it should be noted that three background plasma densities have been chosen so that the ratios of their upper hybrid frequencies to electron gyrofrequency ω_{UH}/Ω_{ce} lie in the bands of $\left(\omega_{UH}^{IR}/\Omega_{ce}, \omega_{2cf}/\Omega_{ce}\right)$, $(\omega_{2cf}/\Omega_{ce}, 5)$, and $(5, 5+\delta)$, respectively, where δ is small positive offset. In Figure 10, the dash curves (a) and (d) are the dispersion curves of the upper hybrid wave and the fifth harmonic of Bernstein wave of irregularity N_1, respectively. The solid curves (b), (c), and (e) are the dispersion curves of the upper hybrid wave of three background plasma, respectively, then their upper hybrid frequencies ω_{UH} will lie in the bands of $\left(\omega_{UH}^{IR}, \omega_{2cf}\right)$, $(\omega_{2cf}, 5\Omega_{ce})$ and $(5\Omega_{ce}, 5\Omega_{ce}+\delta)$ corresponding to the cases of LB, GB, and HB, respectively. Moreover, the following convention is adopted in Figure 10: the part of the dispersion curve between the upper hybrid cutoff $k = 0$ and the second cutoff $k = k_{2cf}$, is termed upper hybrid mode, while that on $k > k_{2cf}$ is termed electron Bernstein mode [*Mjolhus*, 1993]. When the pump is operated at a particular frequency in band $\left(\omega_{UH}^{IR}, \omega_{2cf}\right)$, the upper hybrid resonance ω_{UH} will be excited in N_0 as shown on curve (b). At the edge of N_1, those upper hybrid resonances will be linearly converted into the upper hybrid wave and propagate into N_1 and be trapped by N_1, furthermore, dissipate energy through Ohmic and heat electrons in N_1. Then the escape of heated electrons from N_1 will take place and result in the increase in the depth of N_1. This implies the decrease in the average electron density in heated region. With regard to the experiment reported in this paper, the second cutoff frequency $f_{2cf} = \omega_{2cf}/2\pi$ should be ~6.848598 MHz in the first cycle.

It is unfortunate that the similar decrease in N_e/N_{e0} cannot be seen obviously in the second, third, and fourth cycles in Figure 6. This may be due to (1) the lower electron density of background ionosphere in the second, third, and fourth cycles than that in the first cycles, (2) the electron density variation both in time and space [*Rietveld et al*., 2003], (3) the relatively small change in artificial electron density [*Rietveld et al*., 2003], (4) the difficulty to measure the relatively small change in artificial electron density using EISCAT UHF radar, and (5) the short integrating time of 10 s.

3.4. Electron Temperature

Although the enhancement in electron temperature by a pump at a single fixed frequency is commonly observed with O mode heating, the magnitude of the enhancement presented here is a function of pump frequency f_{HF} as shown by formula (2). The mechanism of second cutoff given by *Mjolhus* [1993] plays a decisive role in the anomalous absorption of the pump. At upper hybrid resonance altitude of the pump, an irregularity N_1 satisfying the condition [*Dysthe et al*., 1982]

$$\Delta N/N_0 > (\lambda/l)^2 \tag{12}$$

can trap the upper hybrid wave excited by the pump, where $\Delta N = N_0 - N_1$ is the characteristic depth of the irregularity, l the scale of variation of N_1, $\lambda^2 = 3\lambda_D^2/\left(1-4Y^2\right)$, and $Y = f_{ce}/f_{HF}$ and give rise to a standing upper hybrid wave, which can heat effectively electron and force out plasma and furthermore deepen the irregularity. With regard to the experiment in this paper, $\lambda \approx 0.0083$ m can be obtained through the measurements of UHF radar, and $l \approx 1$ m is putted for the typical ionosphere [*Dysthe et al*., 1982; *Mjolhus*, 1993], then $(\lambda/l)^2 \approx 6.87 \times 10^{-5}$. Indeed, the ionospheric heating can generate a broad spectrum of density irregularities in the heated region, then the condition should be satisfied regularly for $\Delta N/N_0 > 6.87 \times 10^{-5}$.

In the LB, namely, in the band of $\left(\omega_{UH}^{IR}, \omega_{2cf}\right)$ shown by the curve (b) in Figure 10, the upper hybrid resonance $\omega_{UH} = \omega_{HF} = \sqrt{\omega_{pe}^2 + \Omega_{ce}^2}$ in N_0 enhanced by the pump may be linearly converted into the upper hybrid wave with a wave number k in N_1, which can be trapped by N_1 and dissipate energy in N_1 through Ohmic. The heated electron may escape from N_1 to balance the thermal pressure of N_1 and enter into N_0 to enhance effectively the average temperature of N_0. The escape of heated electrons will deepen N_1 and reduce the cooling rate of N_1 due to the poor thermal coupling between the lower density plasma and the neutral atmosphere.

Similarly, in the HB where the pump sweeps in the band of $(5\Omega_{ce}, 5\Omega_{ce}+\delta)$ as shown by the curve (e) in Figure 10, the dispersion curve of upper hybrid wave in N_0 almost coincide with that of the fifth harmonic of Bernstein wave in N_1 for small wave number. Strictly, the upper hybrid resonance enhanced by the pump in N_0 can be coupled into the fifth harmonic of Bernstein wave of N_1 and trapped in N_1. Due to the larger phase velocity of the fifth harmonic of Bernstein wave of N_1 in the band of $(5\Omega_{ce}, 5\Omega_{ce}+\delta)$ than that of the upper hybrid wave of N_1 in the band of $\left(\omega_{UH}^{IR}, \omega_{2cf}\right)$, however, the trapped fifth harmonic of Bernstein wave will dissipate less energy through Ohmic into N_1 in the band of $(5\Omega_{ce}, 5\Omega_{ce}+\delta)$. Thus, in N_1, the cooling rate in the band of $(5\Omega_{ce}, 5\Omega_{ce}+\delta)$ should be larger than that in the band of $\left(\omega_{UH}^{IR}, \omega_{2cf}\right)$, then $(T_e/T_{e0})_{LB} > (T_e/T_{e0})_{HB}$ is led to.

However, the above mechanism will cease to work when the pump frequency ω_{HF} approaches $5\Omega_{ce}$. In other words, there will be an abrupt disappearance of the enhancement in electron temperature once the pump frequency ω_{HF} passes $5\Omega_{ce}$ from above, and then a gradual recovery of the enhancement in electron temperature as the frequency is further stepping down. When the pump is operated in the band of $(\omega_{2cf}, 5\Omega_{ce})$ as shown by the curve (c), that is, in the GB, the upper hybrid resonance excited by the pump in N_0 cannot be linearly converted into the upper hybrid wave in N_1. In other words, the trapping of upper hybrid wave will not take place in N_1, then N_1 will not develop, and electron will not be heated effectively.

The frequency bandwidth $m\Omega_{ce} - \omega_{HF}$ for the disappearance of enhancement in electron temperature can be estimated by [*Mjolhus*, 1993]

$$(m\Omega_{ce} - \omega)/\omega \approx K_m (\Delta N/N_0)^{m-2} \quad m = 3, 4, 5, \ldots \tag{13}$$

where

$$K_m = (m-1)^{m-1}/(m-2)^{m-2} \times \widetilde{C}_m/\widetilde{B}_m^{m-1},$$
$$\widetilde{B}_m = 3/(m^2-4),$$
$$\widetilde{C}_m = (m^2-1)/m^2 \times \left(Y^2 2^m m!\right)^{-1}.$$

Considering the GB of [6.84299 MHz, 6.857009 MHz] in the third cycle, $K_5 \approx 137$, $(5\Omega_{ce} - \omega_{HF})/\omega_{HF} \approx 0.002$ and $\Delta N/N_0 \approx 2.48\,\%$ can be obtained, which are in perfect agreement with the theoretic estimation given by *Mjolhus* [1993, Table 1]. In other words, for the irregularity of $\Delta N/N_0 \approx 2.48\,\%$, the enhancement in electron temperature will disappear once $(5\Omega_{ce} - \omega_{HF})/\omega_{HF} \approx 0.002$ when the pump frequency ω_{HF} approaches $5\Omega_{ce}$ from below.

4. Conclusions

This paper reports the experimental phenomena involving the apparent enhancement in electron temperature and electron density during an ionospheric heating experiment with a frequency near the fifth electron gyrofrequency on 11 March 2014 at EISCAT Tromsø site in northern Norway.

The UHF incoherent scatter radar observation shows some strong enhancements in electron density when the pump is operating slightly above the fifth electron gyrofrequency, which extends from approximately the reflection altitude of the pump to the limit of the radar measurement above 700 km and are apparently altitude independent. Although the observations of plasma line spectrum show no true increase in electron density, those strong apparent enhancements in electron density are corresponding to the enhancements in ion line or radar echo and consistent temporally with the upshifting and spread of plasma line at frequencies slightly above pump frequency around the reflection altitude of the pump. To our knowledge, the four-wave interaction, strong Langmuir turbulence, and Langmuir waves scattering off the lower hybrid density fluctuations suggested by *Borisova et al*. [2016], *DuBois et al*. [1988, 1990, 1991, 1993], and *Kuo and Lee* [1992], respectively, cannot explain completely the upshifting and spread of plasma line. It seems that many processes may compete with each other and much more work remains to be done.

In addition, the observations also show some enhancements in electron temperature occurring near the reflection altitude of the pump, which appear to be a function of pump frequency. Due to the low cooling rate induced by the escape of thermal electron, the strongest enhancement occurs below the fifth electron gyrofrequency. The second strongest occurring above the fifth electron gyrofrequency is due to the trapped fifth harmonic of Bernstein wave with a larger phase velocity, whereas those enhancements in electron temperature at the pump frequency very close to the fifth electron gyrofrequency are much less than those both below and above the fifth electron gyrofrequency, due to the absence of the trapping of upper hybrid waves.

Acknowledgments

We would like to thank the engineers of EISCAT in Tromsø for keeping the facility in excellent working condition and Tromsø Geophysical Observatory, UiT the Arctic University of Norway, for providing the magnetic data for Tromsø recorded on 11 March 2014. The data of UHF radar and the vertical profile of the electron density above EISCAT at the beginning and during the experiment from the ionosonde can be obtained from EISCAT http://www.eiscat.se/schedule/schedule.cgi and http://dynserv.eiscat.uit.no/DD/login.php, respectively. The EISCAT Scientific Association is supported by China (China Research Institute of Radiowave Propagation), Finland (Suomen Akatemia of Finland), Japan (the National Institute of Polar Research of Japan and Institute for Space-Earth Environmental Research at Nagoya University), Norway (Norges Forkningsrad of Norway), Sweden (the Swedish Research Council), and the UK (the Natural Environment Research Council).

References

Baumjohann, W., and R. A. Treumann (1997), *Basic Space Plasma Physics*, Imperial College Press, London.

Bernhardt, P. A., M. Wong, J. D. Huba, B. G. Fejer, L. S. Wagner, J. A. Goldstein, C. A. Selcher, V. L. Frolov, and E. N. Sergeev (2000), Optical remote sensing of the thermosphere with HF pumped artificial airglow, *J. Geophys. Res.*, *105*, 10,657–10,671, doi:10.1029/1999JA000366.

Blagoveshchenskaya, N. F., T. D. Borisova, M. T. Rietveld, T. K. Yeoman, D. M. Wright, M. Rother, H. Luhr, E. V. Mishin, and C. Roth (2011a), Results of Russian experiments dealing with the impact of powerful HF radio waves on the high-latitude ionosphere using the EISCAT facilities, *Geomagn. Aeron.*, *51*, 1109–1120, doi:10.1134/S0016793211080160.

Blagoveshchenskaya, N. F., T. D. Borisova, T. K. Yeoman, M. T. Rietveld, I. M. Ivanova, and L. J. Baddeley (2011b), Artificial small-scale field aligned irregularities in the high latitude *F* region of the ionosphere induced by an X-mode HF heater wave, *Geophys. Res. Lett.*, *38*, L08802, doi:10.1029/2011GL046724.

Borisova, T. D., N. F. Blagoveshchenskaya, A. S. Kalishin, M. Kosch, A. Senior, M. T. Rietveld, T. K. Yeoman, and I. Hagstrom (2014), Phenomena in the high-latitude ionospheric *F* region induced by a HF heater wave at frequencies near the fourth electron gyroharmonic, *Radiophys. Quantum Electron.*, *57*(1), 1–19, doi:10.1007/s11141-014-9489-6.

Borisova, T. D., N. F. Blagoveshchenskaya, A. S. Kalishin, M. T. Rietveld, T. K. Yeoman, and I. Hagstrom (2016), Modification of the high-latitude ionospheric *F* region by high-power HF radio waves at frequencies near the fifth and sixth electron gyroharmonics, *Radiophys. Quantum Electron.*, *58*(8), 561–585, doi:10.1007/s11141-016-9629-2.

Bryers, C. J., M. J. Kosch, A. Senior, M. T. Rietveld, and T. K. Yeoman (2013), The thresholds of ionospheric plasma instabilities pumped by high-frequency radio waves at EISCAT, *J. Geophys. Res. Space Physics*, *118*, 7472–7481, doi:10.1002/2013JA019429.

Djuth, F. T., B. Thidé, H. M. Ierkic, and M. P. Sulzer (1987), Large *F* region electron-temperature enhancements generated by high-power HF radio waves, *Geophys. Res. Lett.*, *14*, 953–956, doi:10.1029/GL014i009p00953.

Dubois, D. F., H. Rose, and D. Russell (1988), Power spectra of fluctuations in strong Langmuir turbulence, *Phys. Rev. Lett.*, *61*(19), 2209–2212, doi:10.1103/PhysRevLett.61.2209.

Dubois, D. F., H. Rose, and D. Russell (1990), Excitation of strong Langmuir turbulence in plasmas near critical density: Application to HF heating of the ionosphere, *J. Geophys. Res.*, *95*(A12), 21,221–21,272, doi:10.1029/JA095iA12p21221.

Dubois, D. F., H. Rose, and D. Russell (1991), Coexistence of parametric decay cascades and caviton collapse at subcritical densities, *Phys. Rev. Lett.*, *66*(15), 1970–1973, doi:10.1103/PhysRevLett.66.1970.

Dubois, D. F., F. Hanssen, H. Rose, and D. Russell (1993), Space and time distribution of HF excited Langmuir turbulence in the ionosphere: Comparison of theory and experiment, *J. Geophys. Res.*, *98*(A10), 17,543–17,567, doi:10.1029/93JA01469.

Duncan, L. M., J. P. Sheerin, and R. A. Behnke (1988), Observations of ionospheric cavities generated by high-power radio waves, *Phys. Rev. Lett.*, *61*, 239–242, doi:10.1103/PhysRevLett.61.239.

Dysthe, K. B., E. Mjølhus, H. Pécseli, and K. Rypdal (1982), Thermal cavitons, *Phys. Scr.*, *T2/2*, 548–559, doi:10.1088/0031-8949/1982/T2B/040.
Gordon, W. E., and H. C. Carlson Jr. (1974), Arecibo heating experiments, *Radio Sci.*, *9*, 1041–1047, doi:10.1029/RS009i011p01041.
Gordon, W. E., H. C. Carlson, and R. L. Showen (1971), Ionospheric heating at Arecibo: First tests, *J. Geophys. Res.*, *76*, 7808–7813, doi:10.1029/JA076i031p07808.
Gurevich, A. V., and G. M. Milikh (1997), Artificial airglow due to modifications of the ionosphere by powerful radio waves, *J. Geophys. Res.*, *102*, 389–394, doi:10.1029/96JA02916.
Gurevich, A. V., A. V. Lukyanov, and K. P. Zybin (1995), Stationary state of isolated striations developed during ionospheric modification, *Phys. Lett. A*, *206*, 247–259, doi:10.1016/0375-9601(95)00595-T.
Gurevich, A. V., A. V. Lukyanov, and K. P. Zybin (1996), Anomalous absorption of powerful radio waves on the striations developed during ionospheric modification, *Phys. Lett. A*, *211*, 363–372, doi:10.1016/0375-9601(95)00970-1.
Gurevich, A. V., T. Hagfors, H. Carlson, A. V. Lukyanov, and K. P. Zybin (1998), Electron temperature measurements by incoherent scattering in the presence of strong small scale temperature irregularities, *Phys. Lett. A*, *246*, 335–340, doi:10.1016/S0375-9601(98)00422-8.
Gurevich, A. V., H. Carlson, M. Kelley, T. Hagfors, A. Karashtin, and K. P. Zybin (1999), Nonlinear structuring of the ionosphere modified by powerful radio waves at low latitudes, *Phys. Lett. A*, *251*, 311–321, doi:10.1016/S0375-9601(98)00786-5.
Gustavsson, B., et al. (2001), First tomographic estimate of volume distribution of HF-pump enhanced airglow emission, *J. Geophys. Res.*, *106*, 29,105–29,124, doi:10.1029/2000JA900167.
Honary, F., A. J. Stocker, T. R. Robinson, T. B. Jones, N. M. Wade, P. Stubbe, and H. Kopka (1993), EISCAT observations of electron temperature oscillations due to the action of high power HF radio waves, *J. Atmos. Terr. Phys.*, *55*(10), 1433–1448, doi:10.1016/0021-9169(93)90109-C.
Honary, F., A. J. Stocker, T. R. Robinson, T. B. Jones, and P. Stubbe (1995), Ionospheric plasma response to HF radio waves operating at frequencies close to the third harmonic of the electron gyrofrequency, *J. Geophys. Res.*, *100*, 21,489–21,502, doi:10.1029/95JA02098.
Kohl, H., H. Kopka, P. Stubbe, and M. T. Rietveld (1993), Introduction to ionospheric heating experiments at Tromsø-II. Scientific problems, *J. Atmos. Terr. Phys.*, *55*, 601–613, doi:10.1016/0021-9169(93)90008-M.
Kosch, M. J., M. T. Rietveld, A. J. Kavanagh, C. Davis, T. Yeoman, F. Honary, and T. Hagfors (2002), High-latitude pump-induced optical emissions for frequencies close to the third electron gyro-harmonic, *Geophys. Res. Lett.*, *29*(23), 2112, doi:10.1029/2002GL015744.
Krasnosel'skikh, V. V., and V. I. Sotnikov (1977), Plasma-wave collapse in a magnetic field, *Sov. J. Plasma Phys.*, *3*(4), 491–495.
Kuo, S. P. (2001), Cascade of the parametric decay instability in ionospheric heating experiments, *J. Geophys. Res.*, *106*, 5593–5597, doi:10.1029/2000JA000240.
Kuo, S. P., and F. T. Djuth (1988), A thermal instability for the spread-*F* echoes from HF-heated ionosphere, *Geophys. Res. Lett.*, *15*(12), 1345–1348, doi:10.1029/GL015i012p01345.
Kuo, S. P., and M. C. Lee (1992), A source mechanism producing HF-induced plasma lines (HFPLS) with up-shifted frequencies, *Geophys. Res. Lett.*, *19*(3), 249–252, doi:10.1029/92GL00092.
Kuo, S. P., and M. C. Lee (1999), On the generation of a broad downshifted spectrum of HF wave enhanced plasma lines in the ionospheric heating experiments, *Geophys. Res. Lett.*, *26*(21), 3289–3292, doi:10.1029/1999GL003652.
Kuo, S. P., and M. Rubinraut (2005), Generation of energetic electrons at second harmonic cyclotron resonance in ionospheric HF heating experiments, *Geophys. Res. Lett.*, *32*, L19102, doi:*10.1029/2005GL023186*.
Kuo, S. P., B. R. Cheo, and M. C. Lee (1983), The role of parametric decay instabilities in generating ionospheric irregularities, *J. Geophys. Res.*, *88*(A1), 417–423, doi:10.1029/JA088iA01p00417.
Kuo, S. P., M. C. Lee, and S. C. Kuo (1985), A theoretical model of artificial spread F echoes, *Radio Sci.*, *20*(3), 546–552, doi:10.1029/RS020i003p00546.
Lehtinen, M., and A. Huuskonen (1996), General incoherent scatter analysis and GUISDAP, *J. Atmos. Terr. Phys.*, *58*(1), 435–452, doi:10.1016/0021-9169(95)00047-X.
Leyser, T. B., B. U. E. Brandstrom, B. Gustavsson, A. Steen, F. Honary, M. T. Rietveld, T. Aso, and M. Ejiri (2000), Simultaneous measurements of high-frequency pump-enhanced airglow and ionospheric temperatures at auroral latitudes, *Adv. Pol. Upper Atmos. Res.*, *14*, 1–11.
Mantas, G. P. (1994), Large 6300-A° airglow intensity enhancements observed in ionosphere heating experiments are excited by thermal electrons, *J. Geophys. Res.*, *99*, 8993–9002, doi:10.1029/94JA00347.
Mantas, G. P., and H. C. Carlson (1996), Reinterpretation of the 6300-A° airglow enhancements observed in ionosphere heating experiments based on analysis of Platteville, Colorado, data, *J. Geophys. Res.*, *101*, 195–209, doi:10.1029/95JA02760.
Mantas, G. P., H. C. Carlson Jr., and C. H. LaHoz (1981), Thermal response of the *F* region ionosphere in artificial modification experiments by HF radio waves, *J. Geophys. Res.*, *86*, 561–574, doi:10.1029/JA086iA02p00561.
Mjolhus, E. (1993), On the small scale striation effect in ionospheric radio modification experiments near harmonics of the electron gyro frequency, *J. Atmos. Terr. Phys.*, *55*, 907–918, doi:10.1016/0021-9169(93)90030-3.
Mjolhus, E., and T. Fla (1984), Direct access to plasma resonance in ionospheric radio experiments, *J. Geophys. Res.*, *89*(A6), 3921–3928, doi:10.1029/JA089iA06p03921.
Najmi, A., B. Eliasson, X. Shao, G. M. Milikh, and K. Papadopoulos (2016), Simulations of ionospheric turbulence produced by HF heating near the upper hybrid layer, *Radio Sci.*, doi:10.1002/2015RS005866.
Newman, A. L., H. C. Carlson Jr., G. P. Mantas, and F. T. Djuth (1988), Thermal response of the *F* region ionosphere for conditions of large HF-induced electron-temperature enhancements, *Geophys. Res. Lett.*, *15*, 311–314, doi:10.1029/GL015i004p00311.
Pedersen, T. R., and H. C. Carlson (2001), First observations of HF heater-produced airglow at the high frequency active auroral research facility: Thermal excitation and spatial structuring, *Radio Sci.*, *36*, 1013–1026, doi:10.1029/2000RS002399.
Ponomarenko, P. V., T. B. Leyser, and B. Thidé (1999), New electron gyroharmonic effects in HF scatter from pump-excited magnetic field-aligned ionospheric irregularities, *J. Geophys. Res.*, *104*, 10,081–10,087, doi:10.1029/1999JA900039.
Rietveld, M. T., and A. Senior (2015), Do ionospheric irregularities focus UHF radar waves? 17th International EISCAT symposium 14–18 Sep., Hermanus, RSA.
Rietveld, M. T., H. Kohl, H. Kopka, and P. Stubbe (1993), Introduction to ionospheric heating at Tromsø-I. Experimental overview, *J. Atmos. Terr. Phys.*, *55*(4/5), 577–599, doi:10.1016/0021-9169(93)90007-L.
Rietveld, M. T., M. Kosch, and N. Blagoveshchenskaya (2003), Ionospheric electron heating, optical emissions, and striations induced by powerful HF radio waves at high latitudes: Aspect angle dependence, *J. Geophys. Res.*, *108*(A4), 1141–1156, doi:10.1029/2002JA009543.
Rietveld, M. T., A. Senior, J. Markkanen, and A. Westman (2016), New capabilities of the upgraded EISCAT high-power HF facility, *Radio Sci.*, *51*, 1533–1546, doi:10.1002/2016RS006093.
Rishbeth, H., and A. Van Eyken (1993), EISCAT: Early history and the first ten years of operation, *J. Atmos. Terr. Phys*, *55*(4–5), 525–542, doi:10.1016/0021-9169(93)90002-G.
Risthbeth, H., and K. Owen (1969), *Introduction to Ionospheric Physics*, Academic Press, New York.

Robinson, T. R. (1989), The heating of the high latitude ionosphere by high power radio waves, *Phys. Rep.*, *179*(2–3), 79–209, doi:10.1016/0370-1573(89)90005-7.

Robinson, T. R., F. Honary, A. J. Stocker, T. B. Jones, and P. Stubbe (1996), First EISCAT observations of the modification of *F* region electron temperatures during RF heating at harmonics of the electron gyrofrequency, *J. Atmos. Terr. Phys.*, *58*, 385–395, doi:10.1016/0021-9169(95)00043-7.

Senior, A., M. T. Rietveld, I. Haggstrom, and M. J. Kosch (2013), Radio-induced incoherent scatter ion line enhancements with wide altitude extents in the high-latitude ionosphere, *Geophys. Res. Lett.*, *40*, 1669–1674, doi:10.1002/grl.50272.

Sotnikov, V. I., V. D. Shapiro, and V. I. Shevchenko (1978), Macroscopic consequences of collapse at the lower hybrid resonance, *Sov. J. Plasma Phys.*, *4*(2), 252–257.

Stocker, A. J., F. Honary, T. R. Robinson, T. B. Jones, P. Stubbe, and H. Kopka (1992), EISCAT observations of large scale electron temperature and electron density perturbations caused by high power HF radio waves, *J. Atmos. Terr. Phys.*, *54*, 1555–1572, doi:10.1016/0021-9169(92)90163-F.

Stubbe, P., H. Kopka, B. Thidé, and H. Derblom (1984), Stimulated electromagnetic emission: A new technique to study the parametric decay instability in the ionosphere, *J. Geophys. Res.*, *89*(A9), 7523–7536, doi:10.1029/JA089iA09p07523.

Stubbe, P., H. Kohl, and M. T. Rietveld (1992), Langmuir turbulence and ionospheric modification, *J. Geophys. Res.*, *97*(A5), 6285–6297, doi:10.1029/91JA03047.

Utlaut, W. F., and E. J. Violette (1974), A summary of vertical incidence radio observations of ionospheric modification, *Radio Sci.*, *9*(11), 895–903, doi:10.1029/RS009i011p00895.